NASA CR-132535

PHYSICAL AND DYNAMICAL STUDIES OF METEORS

Contract NAS 1-11204

Special Progress Report

1 February to 30 November 1973

Principal Investigators

Richard B. Southworth
Zdenek Sekanina

June 1974

(NASA-CR-132534) PHYSICAL AND DYNAMICAL STUDIES OF METEORS Special Progress Report, 1 Feb. - 30 Nov. 1973 (Smithsonian Astrophysical Observatory) 38 p HC $3.75 CSCL 03B G3/91

N75-10891

Unclas 53194

Prepared for

National Aeronautics and Space Administration
Langley Research Center
Langley Station
Hampton, Virginia 23365

Smithsonian Institution
Astrophysical Observatory
Cambridge, Massachusetts 02138

406-057

1. Report No. NASA CR-132535	2. Government Accession No.	3. Recipient's Catalog No.
4. Title and Subtitle PHYSICAL AND DYNAMICAL STUDIES OF METEORS		5. Report Date NOVEMBER 1974
		6. Performing Organization Code
7. Author(s) Richard B. Southworth and Zdenek Sekanina		8. Performing Organization Report No.
9. Performing Organization Name and Address Smithsonian Institution, Astrophysical Observatory Cambridge, Massachusetts 02138		10. Work Unit No. 188-45-52-03
		11. Contract or Grant No. NAS1-11204
12. Sponsoring Agency Name and Address National Aeronautics and Space Administration Washington, DC 20546		13. Type of Report and Period Covered Contractor Report
		14. Sponsoring Agency Code

15. Supplementary Notes

This is a topical report

16. Abstract

Distribution of meteors in streams detected in the synoptic-year meteor sample plus a study of the fragmentation characteristics of the synoptic-year meteor sample are presented. Population coefficients and dispersion coefficients were determined for each meteor stream. These two parameters serve to determine the number of definite members of the stream in the sample used, and to estimate the actual space density of meteor streams. From results of the fragmentation study, it appears that the main body of most radar meteors does not ablate fragments layer by layer, but collapses rather suddenly under dynamic pressures on the order of 2×10^{-4} dynes cm^{-2}. Furthermore, it is believed that fragmentation does not cause a serious selection effect in the radar meteor data.

17. Key Words (Suggested by Author(s))	18. Distribution Statement
meteor; radar observation, distributions; selection effects; space density; fragmentation; meteor streams; luminosity; recombination; diffusion; meteor masses; orbital parameters; simultaneous observation; image orthicon	Unclassified - Unlimited

19. Security Classif. (of this report)	20. Security Classif. (of this page)	21. No. of Pages	22. Price*
Unclassified	Unclassified	35	$3.25

*For sale by the National Technical Information Service, Springfield, Virginia 22151

TABLE OF CONTENTS

PHYSICAL AND DYNAMICAL STUDIES OF METEORS

Special Progress Report

1. SPACE DENSITY AND COLLISIONS OF METEOROIDS

A revised version of Sections 6 and 7 of our previous Special Progress Report (NASA CR-2316) is being prepared for journal publication.

A general theoretical investigation of space density of meteoroids, which takes collisions, the Poynting-Robertson effect, and sources into account, has been formulated. It will be carried further when the observational bias resulting from fragmentation has been quantitatively assessed.

2. FRAGMENTATION

2.1 Significance of Fragmentation

Jacchia (1955) showed that mass ablation in the form of small particles, rather than in that of individual molecules, predominates in the fainter photographic (Super-Schmidt) meteors. Fragmentation of this sort was, naturally, expected in radar meteors; finally, Southworth (1973) showed that it is common in the Havana radar meteors. Theoretical treatments of the physical interaction of the meteoroid with the atmosphere have not yet, however, properly come to grips with the physics of fragmentation.

A study of fragmentation was included in the present program of research for several reasons: The synoptic-year data, because of the careful calibration of the Havana recording apparatus, contains more information on radar meteor fragmentation than has hitherto been available. A better understanding of the physical interaction is essential for proper interpretation of the observations, especially as regards selection effects (the possible drastic selection effect that depends on fragmentation is discussed below). Finally, we hope to learn more about the physical nature of the meteoroid before it enters the atmosphere.

The present discussion is of the nature of an interim report on an uncompleted study. It will, however, permit some useful conclusions to be accepted temporarily.

2.2 Data

This report uses the condensed results of the synoptic-year reductions; specifically, some of the results for each meteor that were originally designed to be punched on "height-density cards," and that are now on tape. The detailed results for individual meteors, originally designed to be printed, have not been used because the computer programing to transform tape designed for printing to tapes suitable for machine reading is not yet complete.

From the synoptic year, 3550 meteors with well-defined decelerations and ionization curves were selected.

As usual in this project, linear electron densities in the ionized column have been denoted by radar magnitudes as defined by Kaiser's (1955) relation,

$$M = 35 - 2.5 \log_{10} q \quad , \tag{1}$$

where q is electrons per centimeter. The computer performs a least-squares fit of the magnitudes M_i deduced from the initial Fresnel zones at stations i and the times t_i of crossing the specular reflection points to a quadratic

$$M_i = a\, t_i^2 + b\, t_i + c \quad , \tag{2}$$

which represents the ionization curve. If this curve indicates a maximum of ionization (rather than a minimum) and if the distribution of stations along the ionization curve reached close enough to the ends (defined by the limiting observable magnitude), the curve is taken to be well defined. The beginning and end heights above sea level h_B and h_E are defined by the points where the ionization curve reached limiting magnitude. The height of maximum ionization h_M is halfway between h_B and h_E, since the observations would only rarely admit a more elaborate form than equation (2). Decelerations were taken to be well defined if positive, and larger than 0.4 of their standard errors. Diffusion rates were also required to be consistent between observations at different stations.

Preatmospheric masses m_∞ have been revised from the computer outputs, by using the ionizing efficiencies found from simultaneous radar–television observations (Cook et al., 1973). Observed ablation coefficients σ were computed with values at the maximum of the ionization curve

$$\sigma = \frac{\dot{m}_{max}}{(m_{max}\ v_{max}\ \dot{v}_{max})} , \tag{3}$$

where the mass-loss rate $\dot{m}_{max}$ is computed from maximum electron density, and the mass at maximum ionization is taken to be

$$m_{max} = \frac{m_{\infty}}{2} . \tag{4}$$

For use in subsequent analysis, "effective" fragment masses m_f and "effective" numbers of fragments N_f have been computed as follows. The computer output gives the "apparent" density δ of a spherical meteoroid that would experience the observed deceleration on the simplified single-body theory (Hawkins and Southworth, 1958). This has been revised by use of the radar—television ionizing efficiency. (The provisional use in the reductions of CIRA 1961 atmospheric densities and the values $\Gamma = A = 1$ for the drag coefficient and shape factor may require much smaller revisions in the future.) If the meteor is conceptually replaced by N_f equal spherical fragments of density 3.4 g cm^{-3}, which would each exhibit the observed deceleration and which sum to the observed mass, we have

$$N_f = \left(\frac{3.4}{\delta}\right)^2 \tag{5}$$

and

$$m_f = \frac{m_{max}}{N_f} . \tag{6}$$

Density 3.4 is taken here, of course, because it is the approximate value for stony meteorites.

Table 1 includes a variety of data for these 3550 meteors. They have been divided into groups of preatmospheric mass m_{∞} and deceleration $\dot{v}_{max}$ at the point of maximum ionization. ($\dot{v}_{max}$ is not the maximum deceleration, which occurs near the end.) The division into groups of m_∞ is also almost an exact division into groups of velocity v_{max} at the point of maximum ionization, because of the limited dynamic range of the radar receivers, and the very steep dependence of ionizing efficiency on velocity. Successive lines of the table give 1) range of $\dot{v}_{max}$ (km sec^{-2}), 2) range of m_∞(g), 3) fraction of the 3550 meteors with these $\dot{v}$ and m_∞, 4) mean value of v_{max}, 5) mean value of $\dot{v}_{max}$, 6) mean number of Fresnel pattern extrema observed, 7) logarithmic mean of effective mass of a fragment (g), 8) logarithmic mean of effective number of fragments, 9) distribution of mean numbers of extrema: 4 lines show, respectively, the fractions of the group with 5–7, 8–12, 13–19, and 20–30 extrema observed, 10) distribution of logarithms of effective fragment masses: 5 lines show, respectively, the fractions whose logarithm of mass (g) is (> -4), (≤ -4 and > -5), (≤ -5 and > -6), (≤ -6 and > -7), and (≤ -7), 11) distribution of logarithms of effective number of fragments: 5 lines show, respectively, the fractions whose logarithm of effective number of fragments is (<0), (≥0 and <2), (≥2 and <4), (≥4 and <6), and (≥6), 12) height of maximum ionization (km), 13) trail length (km), 14) rise above limiting magnitude $M_{lim} - M_{max}$, 15) maximum magnitude, 16) logarithm of ablation coefficient (cgs). Logarithms are decimal. Groups containing fewer than 10 meteors (less than a fraction 0.0028 of the sample) have not been listed, but are represented in the sum groups. The average of the logarithm of pre-atmospheric mass is not tabulated, but may be found as the sum of the averages of logarithms of effective fragment mass and number of effective fragments. There are no observations of large meteors with large deceleration or small meteors with small deceleration in Table 1. Any analysis of fragmentation needs to explain this absence.

2.3 Height Data

Our observable meteor heights are known to be bounded on the top by diffusion (Southworth, 1973). This is inevitably reflected in the selection of data for Table 1, although the effect is much smaller there than in the total observational sample because high meteors are much less likely to have their deceleration sufficiently well measured for Table 1. An unbiased determination of the trend of heights with velocity can be derived from Figure 4-1 of Southworth and Sekanina (1973). Because the diffusion limit to height increases with velocity, some observations are missed at all velocities but the effect is marked only at the highest velocities. Taking the peaks of the height histograms in Figure 4-1 and adding estimated corrections of 2 km to the height at the highest velocity group and 1 km to the height at the next two velocity groups, we derive Figure 1.

The straight line drawn in Figure 1 corresponds to the following relation between the atmospheric density ρ_{max} at the point of maximum ionization and the velocity v,

$$\rho_{max} \propto v^{-1.9} \quad . \tag{7}$$

2.4 Fresnel Pattern Extrema

Successive maxima and minima (collectively extrema) of the observed Fresnel diffraction patterns are formed by the passage of the head of the ionized column across successively shorter intervals (Fresnel zones) of the trail. The time interval between successive extrema decreases uniformly, and the difference in amplitude decreases monotonically (often until there are no further extrema), so that only a rather well-defined number of extrema can be measured. We will interpret this number in terms of fragmentation, but it is first necessary to discuss other effects.

The computer program that found the extrema rejected data yielding fewer than 5 extrema, and stopped its search at 30. However, extrapolation of the distribution of the mean number of extrema measured per meteor (MEXT in Table 1) shows that the data lost by both limits is relatively small. The loss is not important for the analysis in this report and can be taken into account elsewhere. The computer program also stopped its count of extrema whenever the interval between successive extrema decreased below 1.5 radar pulses, to avoid misidentifications. At the mean velocity and slant range of each of the mass groups in Table 1, this limits the observed number of extrema to the values given in Table 2. The breakdowns of MEXT in Table 1 show that some meteors in each group had more observed extrema than the limit for the mean; these are meteors at greater than mean range or less than mean velocity. Correspondingly, other meteors would have had lower limits to observed extrema. The mean number of observed extrema is significantly below the limit imposed by the 1.5-pulse spacing (and below the limit of 30 extrema). We conclude that the 1.5-pulse spacing limit is responsible for much of the difference in mean number of extrema observed at different masses and velocities, but that other limitations are common.

Diffusion of the ion column into the surrounding atmosphere causes an exponential decay in the smoothed (Fresnel oscillations removed) amplitude, which eliminates extrema after an initial few. We may study this in terms of Loewenthal's (1956) theoretical Fresnel patterns, which depend on his parameter

$$C = \frac{8\pi D\sqrt{\lambda R/2}}{\lambda^2 v} \quad , \tag{8}$$

where D is the diffusion coefficient, λ the radar wavelength, and R the slant range. Within our observed height interval,

$$\log_{10} D(\mathrm{cm}^2\ \mathrm{sec}^{-2}) = 0.068h - 1.67 \quad , \tag{9}$$

where h is height in kilometers. We may take mean slant range to be twice mean height adequately for this purpose. Table 2 also gives C computed by use of mean velocity and height for each group in Table 1. Values of C below 0.29 eliminate no extrema before the 30th, and the values of C just found have no practical effect on the ease of observing any extremum. There are, of course, meteors at greater heights than the mean that are more affected by diffusion, but the restriction in Table 1 to meteors giving good decelerations essentially eliminates all those close to the diffusion ceiling on height. We conclude that diffusion is unimportant in determining the observed numbers of extrema in Table 1.

The remaining possible limitation to observed numbers of extrema is fragmentation. Arbitrary distributions of fragments along the trajectory can give very odd Fresnel patterns, but any reasonably smooth unimodal distribution suppresses, or nearly suppresses, all Fresnel oscillations after the interval between two successive maxima or minima has shrunk to the whole half-width of the fragment distribution. Attributing much of the limitation on extrema to fragmentation, we interpret the width of the last two observed Fresnel zones as a high estimate of the half-width of the fragment spread. If k extrema were observed, the width of the last two zones is, very nearly,

$$w = \sqrt{\frac{R\lambda}{2(k - 3/4)}} \quad , \tag{10}$$

and again we may take R to be twice the height for this purpose. Table 2 gives values of w, computed with mean values of k and height.

2.5 Lag

Observed distances between radar meteor fragments much exceed the fragment diameters and atmospheric mean free paths, and are very nearly parallel to the direction of motion. We infer that the fragments are independent of each other when observed, and that we may neglect any aerodynamic interaction between fragments after their initial separation. It is natural to compare the relative displacements of the fragments along the trajectory with the total displacement of the main body or of the center of the group of fragments caused by the atmosphere. This total displacement will be called the "lag;" it is the distance between the main body (or fragment group) and a hypothetical meteoroid that has experienced no atmospheric deceleration since the fragments separated. A fragment whose mass/cross-section ratio is 1/f of the mass/cross-section of the main body would be expected to have f times the lag of the main body.

The distribution of mass/cross-section among fragments in a group depends on their mass, shape, and density distributions. It cannot be predicted with any certainty, but an attempt (too long to describe here) at a realistic estimate concludes that the standard deviation of mass/cross-section is roughly 0.3 to 0.5 of the mean value.

If separation occurs at t_0, and if $\dot{v}$ is the meteoroid deceleration, the lag at time t is

$$L = -\int_{t_0}^{t} \int_{t_0}^{t_2} \dot{v} \, dt_1 \, dt_2 \quad . \tag{11}$$

The observed values of $\dot{v}_{max}$ in Table 1 were derived by fitting observed velocities v at times t to an expression equivalent to

$$v = v_{max} - \dot{v}_{max} \{\exp [1.4 \, v_{max} \cos Z_R \, H^{-1} (t - t_{max})] - 1\} \quad . \tag{12}$$

Without the factor 1.4, and provided the $\dot{v}_{max}$ term is relatively small, (12) is the theoretical form for the deceleration of a nonablating single meteoroid in an exponential atmosphere. The empirical factor 1.4, adopted from the results of Super-Schmidt meteors, roughly adapts the form to ablation and fragmentation. Nothing more refined is possible with the radar data.

The time of fragment separation is of course unknown, but we will temporarily assume that separation occurs at the beginning of the observed ionized trail. By use of (11) to approximate $\dot{v}$, and neglecting $1 - v/v_{max}$, the lags at the maximum and end of the ionized trail are

$$L_{max} = -\left(\frac{G}{v_{max}}\right)^2 \dot{v}_{max} \left[1 - \left(1 + \frac{g}{2G}\right) \exp\left(\frac{-g}{2G}\right)\right] \tag{13}$$

and

$$L_{end} = -\left(\frac{G}{v_{max}}\right)^2 \dot{v}_{max} \exp\left(\frac{g}{2G}\right) \left[1 - \left(1 + \frac{g}{G}\right) \exp\left(\frac{-g}{G}\right)\right] \quad , \tag{14}$$

where g is the trail length and

$$G = H/1.4 \cos Z_R \tag{15}$$

is the scale distance in which deceleration increases by a factor e. Substituting mean values of $\cos Z_R = 0.7$ and $H = 6$, and $\dot{v}_{max}$ and g from Table 1, we obtain the representative values of L_{max} and L_{end} shown in Table 3.

2.6 Fragmentation Degrades Observed Decelerations

Table 3 also contains the width w of the last two observed Fresnel zones. Taking w as a high estimate of the fragment spread, we expect it to be roughly proportionate to the lag. It is evident, however, that this is not true; the lag (either one) is proportional to deceleration but w is almost independent of deceleration.

We resolve the problem by observing that a group of fragments some 200 m long is not as satisfactory a radar target as the single body on which the analyses have been founded. The centroid of the group will shift within the group as different fragments increase or decrease their electron output. Any spread of the fragments normal to the trajectory, moreover, will have a very large effect on the centroid; we will neglect this effect for the present. The fragments will tend to be arranged in rough order of ablation, the most recently ablated being at the head. If the meteoroid is inhomogeneous in structure, we may expect systematic differences in fragment size within the group, and therefore large shifts in the radar centroid as one subgroup or another flares (subfragments) or burns out.

To estimate a plausible "fragmentation" error in deceleration, consider a 100-m shift of the radar centroid within the 200-m group while one Fresnel pattern is generated (typically 2 to 3 km of trajectory). That pattern would imply a velocity 3 to 5% wrong. The typical drop in velocity between the first and last observed Fresnel patterns is 8%, virtually independent of velocity. In a simple case, where the erroneous velocity is one of only two velocities with significant weight, one at the beginning and one at the end, the centroid shift thus causes a deceleration error of the order of 40 to 60%. There are comparable errors in other cases. A back-and-forth shift of the centroid would obviously cause even larger errors.

Confirmation of the unreality of the "observed" decelerations is given by the near independence of height and deceleration within each mass group of Table 1. Any real physical circumstance causing order-of-magnitude differences in deceleration ought to have more effect on height. We would, furthermore, expect deceleration to be proportional to the cosine of the radiant zenith distance cos Z_R, but that quantity (not tabulated here) shows only the most moderate trend toward larger values at the higher decelerations.

Once the fragmentation error in deceleration is recognized, we see that individual decelerations are of small value and that we should confine further interest in Table 1 to the right-hand column, which is an average of the others. Conversely, being convinced that the scatter in the decelerations is largely unreal, we deduce the probable inhomogeneity of the meteoroids, since $\log_{10}$ (number of fragments) ranges from 0.8 to 1.4 in Table 1, and random electron-output variations among so many fragments would not shift the group centroid enough to cause the observed deceleration scatter.

2.7 Trail Lengths

The 11-km spacing between stations was chosen to obtain well-distributed observations along some of the longer ionized trails we expected to record. This expectation was based on the simplified theory for single-body meteoroids as well as on observed trail lengths for bright radar meteors, but it proved wrong for the faint radar meteors recorded at Havana. These, we found, typically had much shorter trails. Well-distributed observations by five or six stations were indeed common, but only when the meteor's path lay more nearly perpendicular than parallel to the line of five stations.

The simplified single-body theory (Hawkins and Southworth, 1958) made the vertical length of the observable trail, $h_{beg} - h_{end}$, dependent only on the difference between the maximum and limiting magnitudes, $M_{lim} - M_{max}$. Table 4 shows theoretical lengths, observed lengths for faint photographic meteors, and lengths for a sample of 6803 synoptic-year meteors with well-defined ionization curves. A scale height H = 5.4 km is assumed for the theory. The standard deviation of a single radar trail length from the mean is designated σ_l.

Table 4 shows that both photographic and radar trails are much shorter than the simplified theory. The most significant comparison between photographic and radar is for the magnitude difference interval 2—4. In the 0—2 interval, the radar data, unlike the photographic, are closely bunched to $M_{lim} - M_{max} = 2$. When $M_{lim} - M_{max} > 4$, the quadratic fit to the ionization curve is likely to be a poor extrapolation at M_{lim}.

Table 5 and Figure 2 show the relation between vertical trail length and cox Z_R for the same 6803 meteors. Quite unlike the simplified theory, we find that the actual (slant) trail length is much more nearly constant than is the vertical trail length. The data can be fitted approximately by

$$h_{beg} - h_{end} = 10.7 \, (\cos Z_R)^{0.89} \tag{16}$$

(Note added in proof: We have just realized that the result in equation (16) is affected by systematic error, because the radar system is not oriented to observe long trails from meteors with small cos Z_R. Nonetheless, the vertical trail length is still significantly dependent on cos Z_R. Our best present assessment is that the use of (16) in the following section remains valid.)

2.8 Model for the Fragmentation Process

The Super-Schmidt observations introduced the concept of a meteoroid main body gradually shedding fragments (seen as the "wake") and sometimes entirely breaking up into an elongated cloud of fragments (seen as "terminal blending"). We use the same concept here for the radar meteors. Both the main body and fragments are considered to generate light and electrons.

Disentangling the effects of simultaneous fragmentation and ionization will not be easy. It is therefore worth noting that an alternative theory can be formed and to show why it fails. The alternative is to suppose that fragmentation occurs appreciably before ionization, so that single-body theory can be used for the (presumably solid) ionizing fragments. Several authors have treated small single bodies; their ionization curve is shorter at the beginning than the simplified theory because the heated outer layer is most of or all the body, and it may be shorter at the end because of deceleration, but it is not very different from the simplified theory. The ablation of fragments from the main body would be separately treated. It would have been convenient to use single-body theory here as well, in terms of a heat of fragmentation that is much smaller than the heat of vaporization in the usual theory, but that is ruled out by the ionization curves that are so much shorter than solid single-body curves. The ionization curve of the fragment cloud must be at least as long as the curve for a single fragment and, if the fragments are all the same size or random sizes, at least as long as the "fragmentation curve" of the main body. (If large fragments are ablated first, and then smaller ones, it is possible for the fragment cloud's ionization curve to be shorter than the main body's fragmentation curve.) Nonetheless, while this model may be useful in clarifying ideas, it cannot be correct because of the marked dependence (equation 16) of vertical trail length on $\cos Z_R$; this is quite at variance with the trail lengths of solid single fragments.

We therefore turn to a model involving simultaneous fragmentation and ionization. The newly ablated fragments will enter the atmosphere at lower heights than they would have reached in independent fall; this is Öpik's (1958) "abnormal environment." Consequently, they will often have very short ionization curves, resembling the lower ends of normal ionization curves. A schematic ionization curve of the entire assembly of main body and fragments can neglect direct ionization by the main body, which will have a much smaller surface area than the fragments together. Two extreme cases of the model will help to clarify ideas. 1) If the main body breaks completely into many fragments before it has ablated appreciable mass by vaporization, we observe only the fragment cloud, and the ionization curve is that of the fragments, perhaps lacking the beginning. 2) If the main body ablates fragments so deep in the atmosphere that they have only very short ionization curves, the observed ionization curve is essentially the main body's fragmentation curve. The observed deceleration in case 1) is that of the fragments; in

2), that of the main body. In intermediate cases, it will tend to lie between those, but it is not difficult to construct cases (as in Section 2.6) where the observed deceleration is much smaller or larger than either the main body or the fragments.

Our working model for analysis of individual meteors is that our data represents a gradation from nearly case 1) for the low-mass (fast) meteors to nearly 2) for the high-mass (slow) meteors. In either event, the fragmentation curve is short compared to single-body ablation curves and, thus, cannot represent ablation of successive layers of fragments but something closer to a sudden collapse, where ablation of the first few fragments weakens the remaining structure. Only such a collapse combined with very short ionization curves for the fragments can explain the result in equation (16).

Our low-mass (fast) meteors appear to approach case 1) because the observed value of $\sigma \sim 10^{-12}$ matches that observed for large solid meteoroids. The relatively large fragment spread (~0.3 km) also appears to require fragmentation early in the ionization curve. Our high-mass (slow) meteors appear to approach case 2) because their observed $\sigma \sim 10^{-11}$ matches that observed for Super-Schmidt meteors where the main body and "wake" (fragment tail) can be separately observed. The greater trail length of the high-mass meteors is consistent with longer persistence of the main body than in low-mass meteors. The smaller fragment spread (~0.2 km) is also consistent.

2.9 Fragment Mass

Whatever the uncertainty in the fragmentation curve of the main body, we may identify the end of the observed ionization curve with the end of the fragment ionization curves. The simplified single-body theory predicts that the atmospheric density at any definite height interval before the end of the ionization curve, like that at the maximum, obeys

$$\rho \propto v^{-2} m_f^{1/3} \quad , \tag{17}$$

where m is the mass at the same height. Correcting (8) for the difference in trail length between fast and slow meteors, we find the atmospheric density at the end of the ionized curve to be

$$\rho_{end} \propto v^{-2.1} \quad , \tag{18}$$

where the fragment mass, formally, obeys

$$m_f \propto v^{-0.3} \quad . \tag{19}$$

Equation (19) should be regarded with caution. Because of our observational correlation between v and m, (19) could also be, roughly,

$$m_f \propto m^{0.04} \quad , \tag{20}$$

and it is not yet clear that either exponent is significantly different from zero.

Table 1 gives mean effective fragment masses m_f. For the low-mass meteors, case 1) implies that this is the real fragment mass. For case 2), this would be $(\delta/3.4)^2$ m, where the total mass m is essentially the main body mass. For transitional cases, m_f would be somewhere between $(\delta/3.4)^2$ m and the fragment mass, thus considerably above the fragment mass. The values in Table 1 are therefore consistent with our finding that fragment mass is independent of velocity, and we find

$$m_f \sim 10^{-6} \text{ g} \quad . \tag{21}$$

This is, furthermore, consistent with McCrosky's (1958) values of 10^{-4} to 10^{-6} g and Smith's (1954) value of 5×10^{-6} g for the masses of particles released in flares of photographic meteors, especially if equation (20) is correct in suggesting larger fragments from larger meteors.

2.10 Selection Effect of Fragmentation

The simplified theory predicts that deceleration at maximum ionization is nearly independent of velocity,

$$\dot{v}_{max} \approx \frac{3 \cos Z_R}{2H\sigma} \quad , \tag{22}$$

where H is the atmospheric scale height (Hawkins and Southworth, 1958). Similarly, any model where σ is independent of velocity (as seems to be the case for the photographic meteors) predicts a similar result. This implies that slow meteors have vastly larger lags than fast meteors and, therefore, that their fragments should be much further spread along the trajectory. Such a spread, however, also implies some measurable spread across the trajectory, and a loss in radar echo strength that would be an extremely significant selection effect against radar observation of slow, fragmenting meteors. It would also be very difficult to recognize.

The working model described in Section 2.8 eliminates the original cause of worry about a selection effect; there is now no theoretical reason to expect that there should be a large class of meteors invisible to our radar. Practical demonstration that there is no such class is not possible by direct means. Nonetheless, we should expect a gradation from those meteors we can observe to those we cannot; the intermediate class of meteors would have shorter Fresnel patterns. Fortunately, we do not see any such intermediate class in appreciable numbers. The distribution of mean numbers of Fresnel extrema (MEXT) in Table 1 for slow meteors is bunched at high numbers; the tail toward low numbers is well explained by meteors close to the faint limiting magnitude of the system. Thus, we also have no practical reason to expect that many fragmenting meteors are lost.

2.11 Results

Several results from the fragmentation study thus far are important in their own right, and will also serve as the basis for quantitative studies of individual observed meteors.

The spread (whole half-width) of the distribution of fragments along the trajectory averages 0.2 to 0.3 km. The centroid of ion production within that spread shifts significantly and systematically within the life of one meteor (but we have not deduced any systematic trend among meteors). The cause of the shift is probably inhomogeneous structure of the meteoroid. The result of the shift is very large errors in individual measures of deceleration.

The main body of most of our meteors does not ablate fragments layer by layer, but collapses rather suddenly under a dynamic pressure of the order of 2×10^4 dynes cm^{-2}. It is not yet certain whether this is quite independent of mass or velocity, or how much it varies among meteors. Evidently, this is the same class of meteors as those with sudden light-curve beginnings that formed 15% of McCrosky's (1955) Super-Schmidt meteors.

Our working model for these meteors envisages a gradation between two simple models. In case 1), the smallest (fastest) break up early in the observed trail and continue as a group of independent fragments. In case 2), the largest (slowest) are observed in the process of breaking up; the fragments have a relatively short independent existence.

The mean mass of meteoroid fragments is nearly independent of mass or velocity, and is of the order of 10^{-6} g.

Contrary to previous expectations from simplified theory, there is no reason to expect that many slow fragmenting meteors will be unobservable by radar. Moreover, we do not find any significant number that are marginally unobservable. We therefore do not think now that fragmentation causes a serious selection effect in our data.

3. DISTRIBUTION OF METEORS IN THE STREAMS DETECTED IN THE SYNOPTIC-YEAR SAMPLE

3.1 Introduction

The distribution of meteor orbits in the 256 streams of the synoptic-year sample (Southworth and Sekanina 1973) was studied in terms of the D-test, which measures the similarity of two orbits by the differences in their Keplerian elements (Southworth and Hawkins 1963). To express a stream's strength relative to the level of the sporadic background and the degree of dispersion of meteor orbits within the stream, the statistical model of meteor streams (Sekanina 1970) which is based on the D-test, defines two parameters of the D-distribution function of meteor orbits. The two parameters, the population coefficient Λ and the dispersion coefficient σ, also serve to determine the number of definite members of the stream in the sample used (Sekanina 1970), and to estimate the actual space density in meteor streams (Southworth and Sekanina 1973).

3.2 Determination of the Parameters Λ and σ

Until recently, the parameters Λ and σ of the D-distribution function were determined graphically (Sekanina 1970). This method required laborious plotting of the D-distribution curves. To avoid this, a new method has recently been developed.

The theoretical cumulative D-distribution, predicted by the statistical model, has the form:

$$N(D) = c \cdot f\left(\frac{D}{\sigma\sqrt{2}}\right), \qquad (23)$$

where N(D) is the number of meteors with the value of the D-test less or equal to D, C is a constant of proportionality, and

$$f(E) = E^{3.8} + 2.64\Lambda \left[\int_0^E e^{-t^2} dt - Ee^{-E^2} \right] \tag{24}$$

Since the parameters Λ and σ obviously cannot be determined explicitly, an iterative least-squares solution has been preferred, which starts from an arbitrary pair of values for Λ and σ in (23) and calculates differential corrections $\Delta \log\Lambda$ and $\Delta \log\sigma$ (as well as $\Delta \log C$) from

$$\left\| \begin{matrix} \Sigma\Delta\log N \\ \Sigma A_\sigma \Delta\log N \\ \Sigma A_\Lambda \Delta\log N \end{matrix} \right\| = \left\| \begin{matrix} n & \Sigma A_\sigma & \Sigma A_\Lambda \\ \Sigma A_\sigma & \Sigma A_\sigma^2 & \Sigma A_\sigma A_\Lambda \\ \Sigma A_\Lambda & \Sigma A_\sigma A_\Lambda & \Sigma A_\Lambda^2 \end{matrix} \right\| \cdot \left\| \begin{matrix} \Delta\log C \\ \Delta\log\sigma \\ \Delta\log\Lambda \end{matrix} \right\| \tag{25}$$

where

$$A_\sigma = -\frac{3.8E^{3.8}}{f(E)} \left[1 + 1.389\Lambda\, E^{-0.8} e^{-E^2}\right], \tag{26}$$

$$A_\Lambda = \Lambda - \frac{E^{3.8}}{f(E)}$$

and

$$E = \frac{D}{\sigma\sqrt{2}} \,. \tag{27}$$

3.3 Numerical results

Since the actual cumulative distribution of meteors in a stream is a by-product of the main stream-search program, the above differential-correction procedure can work directly with the punched output of the distribution data. Practical calculations have shown that selection of arbitrary constants in the place of the initial values of Λ and σ has created no problems and that in all but six of the 256 cases the procedure converged successfully in less than 70 iterations and in most cases in less than 10 iterations. In four cases (May Arietids, α Draconids, L Cepheids and ε Umids) the method failed to converge, and in two cases (April Ursids and ε Ursids) failed to yield any solution (the reason being that the slope of the D-curve at $D \lesssim 0.1$ was steeper than allowed by the model). In one other case (α Auriqids) the solution did converge, but indicated that this "stream" does not satisfactorily discriminate from the sporadic background.

Table 6 lists the results. An abbreviated name of the stream is given in the first column (an asterisk meaning that the stream was also detected in the 1961-65 sample) the parameters Λ and σ are in the second and third, respectively, the inner and outer limits, D_{I}, D_{II}, of the stream (for definition see Sekanina 1970) in the next two columns, and the number of definite members of the stream in the sample is in the last column. The definite members total 3182, or about 16% of the whole synoptic-year sample. A stream's population averages at about 12 to 13 meteors.

4. ON THE POTENTIAL ASSOCIATION OF FOUR METEOR STREAMS WITH THE MINOR PLANET ADONIS

4.1 The problem

There are four streams in the synoptic year sample with orbits similar to that of the minor planet Adonis: Capricornids-Sagittariids, Scorpiids-Sagittariids, χ Sagittariids and ε Aquarids. In terms of D the difference between the orbit of any of these streams and that of the minor planet is less than 0.2.

The orbital similarity may of course suggest the evolutionary relationship, implying that Adonis might have been a comet long time ago, and the meteor streams could be its debris. In that case the streams should indeed move in orbits similar to, but not identical with that of Adonis. The orbital difference is partly due to the non-zero momentum the ejected particles gained, enhanced by accumulation of differential perturbations by the planets since the time of ejection, partly due to the different size of the parent body and the debris.

4.2 The calculations

We have made an attempt to explore the observed difference between the orbits of Adonis and the orbits of the potentially associated streams to learn something on the time and circumstances of ejection.

Since Adonis has aphelion at 3.3 A.U. and close encounters with Jupiter are excluded, only secular perturbations were considered. Poynting-Robertson effect can be shown to accumulate over the spans of time considered here to not more than 0.09 A.U. in the semi-major axis, which is less than the uncertainty in the semi-major axis of the mean orbits of the streams. The effect of radiation pressure on the ejected particles was considered, although it appears to be less important than the other effects discussed below. For a zero ejection velocity the corrections to the five orbital elements due to radiation pressure are:

$$\Delta\omega_{rp} = -\frac{\sin v}{e}\frac{\Delta k^2}{k^2},$$

$$\Delta\Omega_{rp} = \Delta i_{rp} = 0, \tag{28}$$

$$\Delta q_{rp} = -q\,\frac{\Lambda - \cos v}{1 + e}\frac{\Delta k^2}{k^2},$$

$$\Delta e_{rp} = -(e + \cos v)\frac{\Delta k^2}{k^2},$$

where v is the true anomaly at the time of ejection, and $\Delta k^2/k^2 < 0$ is the relative reduction in the gravitational constant due to radiation pressure, which amounts to

$$\frac{\Delta k^2}{k^2} = -\frac{6 \times 10^{-5}}{\rho_s a_s} Q_{rp}, \tag{29}$$

ρ_s and a_s are the density and radius of the particle, $Q_{rp} \doteq 1$ is the scattering efficiency for radiation pressure. The masses of meteoroids in the considered streams are about 10^{-4}g, which gives typically $\rho_s a_s \simeq 0.03\text{gm}^{-2}$ and therefore $\Delta k^2/k^2 = -0.002$.

There are three other factors, determining the future orbit of an ejected meteoroid: the time of ejection, the position of the ejection point in orbit (involved also in the radiation-pressure effect (28)), and the ejection velocity (both magnitude and direction). If we know both the position of ejection in orbit, given by the true anomaly v, and the velocity of ejection, given by the radial $\dot{\xi}$ and transverse $\dot{\eta}$ components (ejection is assumed to be directed in the orbital plane), we can write for the corrections to the orbital elements of the parent body:

$$\Delta\omega = \frac{C_o}{e}\left[-\dot{\xi}\cos v + \dot{\eta}\,\frac{2 + e\cos v}{1 + e\cos v}\sin v\right],$$

$$\Delta\Omega = \Delta i = 0,$$

$$\Delta q = -\frac{C_o q}{1+e}\left[-\dot{\xi}\sin v + \dot{\eta}\,\frac{1 - \cos v + e\sin^2 v}{1 + e\cos v}\right], \tag{30}$$

$$\Delta e = C_o\left[\dot{\xi}\sin v + \dot{\eta}\,\frac{2\cos v + e(1 + \cos^2 v)}{1 + e\cos v}\right],$$

where

$$C_o = \frac{q^{1/2}(1+e)^{1/2}}{v} \tag{31}$$

and $v = 2.978 \times 10^4$, if $\dot{\xi}$ and $\dot{\eta}$ are expressed in meters per second.

The model calculations started with running the orbit of Adonis back for 12000 years, applying the secular perturbations by Jupiter to Neptune. Based on our previous experience (Sekanina 1971), we assumed ejections to take place at five discrete times 4000 to 12000 years ago, always 2000 years apart. At each time, ejections were considered to take place at 1.2 A.U. and 0.7 AU from the sun before perihelion, at perihelion, and also 0.7 and 1.2 A.U. after perihelion. The ejections were then assumed to be directed toward the sun and also deviating by 30° and by 60° both in and opposite to the direction of motion. Finally, the magnitude of the ejection velocity was estimated from Probstein's (1968) fluid-dynamics model. Assuming that at the time of ejection the radius of Adonis was between 1 and 20 km, the vaporization rate between 1 $\times 10^{17}$ and 7×10^{17} molecules/$cm^2 \cdot$ sec and surface temperature 190° to 200° K (both fitting a range of values for water snow), the minimum ejection velocity, $v_e = (\dot{\xi}^2 + \dot{\eta}^2)^{1/2}$, of meteoroids of $\rho_s a_s = 0.03$ g cm^{-2} would vary as $17/r$ (m sec^{-1}), the maximum velocity as $200/r$ (m sec^{-1}), where r is the heliocentric distance in A.U. A case with $60/r$ (m sec^{-1}) was also considered, assumed to be a reasonable mean value.

4.3 The results

Altogether, therefore, five ejection times were considered with $5 \times 5 \times 3 = 75$ options in each case, or a total of 375 individual models. For each of them the initial orbital elements were computed from the orbital elements of Adonis at the time of ejection, adding the corrections due to radiation pressure

5. REFERENCES

Cook, A. F., Forti, G., McCrosky, R. E., Posen, A., Southworth, R. B., and Williams, J. T., 1973. Combined observations of meteors by image-orthicon television camera and multistation radar. In The Evolutionary and Physical Properties of Meteoroids, Proc. IAU Colloq. No. 13, ed. by A. L. Cook, C. L. Henenway, and P. M. Millman. NASA SP-319, 13.

Hawkins, G. S., and Southworth, R. B., 1958. Smithsonian Contr. Astro-phys., vol. 2, 349.

Jacchia, L. G., 1955. Astrophys. Journ., vol. 121, 521.

Kaiser, T. R., 1955. The interpretation of radio echoes from meteor trails. In Meteors, ed. by T. R. Kaiser, Pergamon Press, London and New York, p. 55.

Loewenthal, M., 1956. Tech. Rep. 132, MIT Lincoln Laboratory, Lexington, Mass.

McCrosky, R. E., 1955. Astron. Journ., vol. 60, 170.

McCrosky, R. E., 1958. Astron. Journ., vol. 63, 97.

Öpik, E. J., 1958. Physics of Meteor Flight in the Atmosphere. Interscience Publ. Inc., New York, p. 62.

Probstein, R. F. 1968. The dusty gasdynamics of comet heads. In Problems of Hydrodynamics and Continuum Mechanics, Philadelphia, p. 568.

Sekanina, Z. 1970. Statistical model of meteor Streams, I. Analysis of the model. Icarus 13, pp. 459-474.

Sekanina, Z. 1971. On the age of a radio meteor stream associated with minor planet Adonis (abstract). Bull. Amer. Astron. Soc. 3, p. 271.

Smith, H. J., 1954. Astrophys. Journ., vol. 119, 438.

Southworth, R. B., and Hawkins, G. S. 1963, Statistics of meteor streams, Smithson. Contrib. Astrophys. 7, pp. 261-285.

Southworth, R. B., 1973. Recombination in radar meteors. In The Evolutionary and Physical Properties of Meteoroids, Proc. IAU Collq. No. 13, ed. by A. F. Cook, C. L. Hemenway, and P. M. Millman. NASA SP-319, 23.

Southworth, R. B., and Sekanina, Z., 1973. Physical and Dynamical Studies of Meteors, NASA CR-2316, 106 pp.

Table 1. Data from 3550 Synoptic Year meteors.

DECEL.	.32-1.0	1.0-3.2	3.2-10.	10.-32.	32.-100.	100.+UP	ALL DECEL.
LOG10 MASS	OVER -2	OVER -2	OVER -2	OVER -2	OVER -2	OVER -2	OVER -2
FRACT	.0197	.0620	.0315	.0025	0.0000	0.0000	.1163
AV VMAX	16.2774	17.6926	18.8872				17.6397
AV DECEL	.6831	1.9578	4.7830				2.7722
AV MEXT	20.7714	20.3046	19.1072				19.9734
AV L FRG M	-1.6002	-2.7070	-3.7759				-2.8434
AV L FRG N	.4277	1.3167	2.1724				1.4292
MEXT 5-7	0.0000	.0045	.0089				.0046
8-12	.1286	.1273	.1429				.1404
13-19	.3857	.3091	.3929				.3414
20-30	.4857	.5591	.4554				.5133
L FRG MASS	.9429	.8500	.5536				.7724
-4 TO -5	.0143	.1000	.2321				.1211
-5 TO -6	.0286	.0318	.1518				.0678
-6 TO -7	.0143	.0136	.0357				.0266
LE -7	0.0000	.0045	.0268				.0121
L FRG NUMB	.4714	.1545	.0536				.1840
0 TO 2	.3857	.5455	.4107				.4697
2 TO 4	.1286	.2727	.4196				.2833
4 TO 6	0.0000	.0227	.1071				.0533
GE 6	.0143	.0045	.0089				.0097
HMAX	87.7200	87.1200	87.1616				87.1823
TRAIL LEN.	11.7609	12.4825	11.6621				12.0930
HMAX-MLIM	3.6700	3.7191	3.8723				3.7700
MAGN(MAX)	11.4986	11.3809	11.2321				11.3380
LOG SIGMA	-10.3914	-10.8744	-11.2345				-10.9034

DECEL.	.32-1.0	1.0-3.2	3.2-10.	10.-32.	32.-100.	100.+UP	ALL DECEL.
LOG10 MASS	-2 TO -3	-2 TO -3	-2 TO -3	-2 TO -3	-2 TO -3	-2 TO -3	-2 TO -3
FRACT	.0093	.0842	.1724	.0293	.0020	0.0000	.2975
AV VMAX	24.0291	24.9598	26.0872	28.0422			25.9091
AV DECEL	.7170	2.1965	5.5707	13.5287			5.6622
AV MEXT	21.1212	20.0301	19.0147	17.1058			19.1278
AV L FRG M	-1.3778	-2.9748	-4.0321	-4.6283			-3.7311
AV L FRG N	-1.0124	.4800	1.4260	1.9022			1.1522
MEXT 5-7	0.0000	.0067	.0098	.0385			.0133
8-12	.0909	.1003	.1225	.1250			.1155
13-19	.2727	.3746	.4085	.5000			.4044
20-30	.6364	.5184	.4592	.3365			.4669
L FRG MASS	.9697	.8595	.4984	.3173			.5947
-4 TO -5	0.0000	.0803	.3105	.3173			.2339
-5 TO -6	0.0000	.0468	.1389	.2308			.1174
-6 TO -7	.0303	.0033	.0327	.0865			.0303
LE -7	0.0000	.0100	.0196	.0481			.0237
L FRG NUMB	.8485	.3478	.1111	.0769			.1979
0 TO 2	.1212	.5753	.6127	.4808			.5691
2 TO 4	0.0000	.0635	.2500	.3942			.2027
4 TO 6	.0303	.0100	.0180	.0385			.0208
GE 6	0.0000	.0033	.0082	.0096			.0095
HMAX	89.4606	90.4421	90.1668	88.3038			90.0635
TRAIL LEN.	12.2667	12.9729	13.2129	11.5472			12.9184
HMAX-MLIM	3.6000	3.6311	3.6745	4.0971			3.7102
MAGN(MAX)	11.3394	11.3896	11.3325	10.9221			11.2989
LOG SIGMA	-10.4339	-10.9464	-11.3548	-11.6897			-11.2480

Table 1. (Cont.)

DECEL.	.32-1.0	1.0-3.2	3.2-10.	10.-32.	32.-100.	100.+UP	ALL DECEL.
LOG10 MASS	-3 TO -4	-3 TO -4	-3 TO -4	-3 TO -4	-3 TO -4	-3 TO -4	-3 TO -4
FRACT	.0023	.0321	.1904	.1496	.0034	0.0000	.3777
AV VMAX	33.1425	31.7109	32.7491	34.7395	35.0267		33.4717
AV DECEL	.8012	2.2738	6.7020	14.9699	48.8558		9.9414
AV MEXT	17.2500	16.3070	15.6805	14.5085	11.5000		15.2416
AV L FRG M	-1.7453	-3.2648	-4.4007	-5.2542	-7.0461		-4.6516
AV L FRG N	-1.5956	-.0486	.9779	1.7148	3.3768		1.1885
MEXT 5-7	0.0000	.0068	.0163	.0132	.0833		.0149
8-12	.1250	.1491	.1938	.2881	.4167		.2269
13-19	.7500	.6404	.6124	.5800	.3333		.6003
20-30	.1250	.2018	.1775	.1186	.1667		.1559
L FRG MASS	1.0000	.7719	.3107	.1318	0.0000		.2804
-4 TO -5	0.0000	.1491	.4201	.2957	0.0000		.3415
-5 TO -6	0.0000	.0702	.2012	.3427	.2500		.2453
-6 TO -7	0.0000	.0088	.0503	.1318	.4167		.0820
LE -7	0.0000	0.0000	.0178	.0979	.3333		.0507
L FRG NUMB	1.0000	.4649	.1627	.0791	0.0000		.1588
0 TO 2	0.0000	.5000	.6864	.5556	.0833		.6092
2 TO 4	0.0000	.0351	.1435	.3164	.6667		.2066
4 TO 6	0.0000	0.0000	.0044	.0377	.1667		.0186
GE 6	0.0000	0.0000	.0030	.0113	.0833		.0067
HMAX	93.0375	92.9000	92.4734	92.3034	93.7167		92.4568
TRAIL LEN.	12.7221	12.0105	11.9524	11.3054	10.0895		11.6891
MMAX-MLIM	3.6500	3.4061	3.4731	3.7228	3.5250		3.5678
MAGN(MAX)	11.2125	11.4974	11.4558	11.2089	11.3917		11.3595
LOG SIGMA	-10.5162	-10.9312	-11.3934	-11.7205	-12.1758		-11.4854

DECEL.	.32-1.0	1.0-3.2	3.2-10.	10.-32.	32.-100.	100.+UP	ALL DECEL.
LOG10 MASS	-4 TO -5	-4 TO -5	-4 TO -5	-4 TO -5	-4 TO -5	-4 TO -5	-4 TO -5
FRACT	0.0000	.0028	.0313	.0879	.0220	0.0000	.1439
AV VMAX		40.5710	43.1657	44.7239	49.8241		45.0827
AV DECEL		2.5140	7.0659	17.8241	48.4267		19.8588
AV MEXT		13.3000	12.1802	11.3269	9.8077		11.3190
AV L FRG M		-3.1816	-4.3703	-5.4793	-6.4697		-5.3446
AV L FRG N		-1.1146	.0161	1.0687	1.8294		.9135
MEXT 5-7		0.0000	.0270	.0417	.1410		.0528
8-12		.3000	.5495	.5705	.5769		.5616
13-19		.5000	.3694	.3333	.2051		.3249
20-30		.2000	.0541	.0545	.0769		.0607
L FRG MASS		.9000	.2613	.0673	.0641		.1252
-4 TO -5		.1000	.5135	.2051	.0385		.2446
-5 TO -6		0.0000	.2162	.4487	.1795		.3483
-6 TO -7		0.0000	0.0000	.2115	.4359		.1957
LE -7		0.0000	.0090	.0673	.2821		.0861
L FRG NUMB		1.0000	.4324	.1218	.1026		.2035
0 TO 2		0.0000	.5586	.7051	.4359		.6184
2 TO 4		0.0000	.0090	.1603	.3974		.1605
4 TO 6		0.0000	0.0000	.0096	.0385		.0117
GE 6		0.0000	0.0000	.0032	.0256		.0059
HMAX		94.4900	94.1775	94.1824	93.7462		94.1207
TRAIL LEN.		10.0275	10.7623	10.2897	8.9274		10.1793
MMAX-MLIM		3.0700	3.3378	3.6003	3.9115		3.5804
MAGN(MAX)		11.7700	11.4712	11.2619	10.8090		11.2481
LOG SIGMA		-10.9140	-11.3782	-11.7539	-12.1253		-11.7126

Table 1. (Cont.)

DECEL.	.32-1.0	1.0-3.2	3.2-10.	10.-32.	32.-100.	100.+UP	ALL DECEL.
LOG10 MASS	-5.LOWER	-5.LOWER	-5.LOWER	-5.LOWER	-5.LOWER	-5.LOWER	-5.LOWER
FRACT	0.0000	0.0000	.0051	.0239	.0318	.0037	.0645
AV VMAX			55.2972	56.4162	58.2167	60.8046	57.4659
AV DECEL			7.4933	19.6926	52.7240	145.2369	42.1600
AV MEXT			9.2778	8.9177	8.4956	8.5385	8.7162
AV L FRG M			-4.6235	-5.6636	-6.5798	-7.7659	-6.1533
AV L FRG N			-.6193	.3398	1.1366	2.1653	.7612
MEXT 5-7			.0556	.1647	.1770	.3077	.1703
8-12			.9444	.6824	.5044	.3846	.5983
13-19			0.0000	.0588	.2212	.3077	.1485
20-30			0.0000	.0941	.0973	0.0000	.0830
L FRG MASS			.0556	.0471	.0265	0.0000	.0349
-4 TO -5			.7778	.1176	.0708	.0769	.1441
-5 TO -6			.1667	.4706	.1062	0.0000	.2402
-6 TO -7			0.0000	.3529	.3982	.1538	.3362
LE -7			0.0000	.0118	.3982	.7692	.2445
L FRG NUMB			.9444	.2824	.1150	.0769	.2402
0 TO 2			.0556	.7059	.7345	.2308	.6419
2 TO 4			0.0000	.0118	.1504	.6154	.1135
4 TO 6			0.0000	0.0000	0.0000	.0769	.0044
GE 6			0.0000	0.0000	0.0000	0.0000	0.0000
HMAX			96.5611	96.1400	94.9230	94.4538	95.4765
TRAIL LEN.			9.8857	9.4502	8.0671	7.5814	8.6958
HMAX-MLIM			3.2167	3.2847	3.3956	3.2308	3.3310
MAGN(MAX)			11.5000	11.4918	11.3726	11.3769	11.4271
LOG SIGMA			-11.3711	-11.7621	-12.1183	-12.5462	-11.9517

DECEL.	.32-1.0	1.0-3.2	3.2-10.	10.-32.	32.-100.	100.+UP	ALL DECEL.
LOG10 MASS	ALL MASS	ALL MASS	ALL MASS	ALL MASS	ALL MASS	ALL MASS	ALL MASS
FRACT	.0313	.1811	.4307	.2932	.0592	.0037	1.0000
AV VMAX	19.7975	23.9131	30.0888	38.7154	52.7705	60.8046	32.6226
AV DECEL	.7017	2.1334	6.1443	16.0626	51.4463	145.2369	11.3403
AV MEXT	20.6216	19.3593	16.9366	13.3698	9.2000	8.5385	15.9625
AV L FRG M	-1.5445	-2.9414	-4.2078	-5.2907	-6.6132	-7.7659	-4.3640
AV L FRG N	-.1463	.6478	1.1561	1.4425	1.6665	2.1653	1.1386
MEXT 5-7	0.0000	.0062	.0144	.0365	.1619	.3077	.0287
8-12	.1171	.1213	.1962	.3900	.5143	.3846	.2566
13-19	.3784	.4012	.4899	.4524	.2333	.3077	.4431
20-30	.5045	.4712	.2995	.1210	.0905	0.0000	.2715
L FRG MASS	.9550	.8414	.3970	.1249	.0381	0.0000	.3930
-4 TO -5	.0090	.0995	.3734	.2546	.0524	.0769	.2572
-5 TO -6	.0180	.0451	.1733	.3727	.1429	0.0000	.2011
-6 TO -7	.0180	.0078	.0379	.1710	.4048	.1538	.0930
LE -7	0.0000	.0062	.0183	.0768	.3619	.7692	.0556
L FRG NUMB	.6216	.3126	.1629	.1085	.1000	.0769	.1851
0 TO 2	.2793	.5428	.6200	.6013	.5619	.2308	.5845
2 TO 4	.0811	.1291	.1949	.2507	.2714	.6154	.2017
4 TO 6	.0090	.0124	.0170	.0307	.0381	.0769	.0214
GE 6	.0090	.0031	.0052	.0086	.0286	0.0000	.0073
HMAX	88.6207	89.8042	91.3329	92.7248	94.3846	94.4538	91.5656
TRAIL LEN.	11.9806	12.5887	12.3249	10.8745	8.5176	7.5814	11.6913
HMAX-MLIM	3.6477	3.6126	3.5701	3.6949	3.6429	3.2308	3.6202
MAGN(MAX)	11.4306	11.4117	11.3917	11.2115	11.1248	11.3769	11.3276
LOG SIGMA	-10.4131	-10.9186	-11.3649	-11.7308	-12.1286	-12.5462	-11.4099

Table 2. Additional data for the mass groups of Table 1.

$\log_{10}$ mass range (g)	> -2	-2 to -3	-3 to -4	-4 to -5	< -5
Limit to number of extrema at mean range and velocity	123	61	37	21	13
Mean observed extrema	20.0	19.1	15.2	11.3	8.7
Loewenthal's C at mean height and velocity	0.039	0.043	0.050	0.047	0.046
Width of last two observed Fresnel zones (km), a high approximation to fragment spread	0.18	0.19	0.22	0.26	0.31

Table 3. Computed lag and width of last two Fresnel zones (km).

	Decel:	0.32–1.0	1.0–3.2	3.2–10	10–32	32–100	100 + up
log m >-2	L_{max}	0.02	0.06	0.12			
	L_{end}	0.14	0.39	0.75			
	w	0.18	0.18	0.18			
-2 to -3	L_{max}	0.01	0.04	0.09	0.16		
	L_{end}	0.08	0.20	0.57	0.92		
	w	0.18	0.18	0.19	0.20		
-3 to -4	L_{max}		0.02	0.06	0.11	0.30	
	L_{end}		0.15	0.36	0.64	1.67	
	w		0.22	0.22	0.24	0.25	
-4 to -5	L_{max}		0.01	0.03	0.07	0.12	
	L_{end}		0.06	0.18	0.39	0.64	
	w		0.23	0.24	0.25	0.27	
≤-5	L_{max}			0.02	0.04	0.09	0.19
	L_{end}			0.10	0.23	0.49	0.95
	w			0.28	0.28	0.29	0.29

Table 4. Mean vertical trail lengths.

	$h_{beg}-h_{end}$ (km)		
$M_{lim}-M_{max}$	Simple theory	Short trail	Synoptic year σ_1
0	0.0		
		7.8	(7.3 ± 2.4)
2	19.0		
		10.4	7.4 ± 2.5
4	29.8		
		18.9	(8.3 ± 2.8)
6	40.0		

Table 5. Mean vertical trail lengths and radiant zenith distance.

$\cos Z_R$	Mean $\cos Z_R$	$h_{beg} - h_{end}$	σ_1
0 to 0.2	0.143	1.71	0.59
0.2 to 0.4	0.318	3.81	1.04
0.4 to 0.6	0.514	6.14	1.90
0.6 to 0.8	0.715	8.07	2.44
0.8 to 1	0.847	8.38	2.53

Table 6

STREAM	LAMBDA	SIGMA	DI	DII	NS
BETA TRIAN	4.3	.066	.118	.167	6
*ZETA AUR	22	.051	.125	.203	6
JAN BOOTID	34	.074	.192	.331	11
TH COR BOR	26	.047	.118	.196	7
LAM BOOTID	560	.018	.062	.168	5
CORONA BOR	21	.056	.141	.228	13
*CANIDS	270	.031	.101	.239	5
*QUADRANT	16	.055	.128	.202	4
JAN SAGIT	420	.025	.064	.217	5
JAN DRACO	77	.032	.092	.178	9
*DEL CANCR	5.2	.072	.135	.193	12
JAN CANCR	5.5	.084	.159	.229	10
PSI LEONID	11	.067	.146	.222	17
XI SAGIT	4.8	.106	.195	.277	16
JAN AQUAR	53	.038	.104	.191	5
*CAPR-SAG	11	.075	.164	.249	14
H DRACONID	96	.029	.085	.170	5
IODTA DRA	28	.053	.134	.225	8
PSI CYGNID	260	.031	.100	.237	5
*ALPHA LEO	4.9	.086	.162	.232	12
LAM CAPR	37	.060	.157	.274	11
*DELTA LEO	5.2	.137	.257	.367	44
EPS AQUAR	6.4	.109	.214	.311	20
FEB DRACO	4.1	.101	.178	.252	32
XI CYGNID	99	.037	.109	.219	8
KAPPA GEM	110	.023	.068	.140	4
RHO LEONID	12	.047	.104	.159	5
MU LEONID	28	.040	.101	.170	5
*PI VIRGIN	13	.056	.130	.201	18
*N ETA VIR	14	.064	.146	.226	10
LEO-URSID	110	.031	.092	.189	3
*S ETA VIR	37	.051	.134	.233	8
MAR HERCUL	440	.026	.068	.228	8
CHI HERCUL	980	.018	.065	.195	5
*S VIRGIN	2.2	.075	.116	.159	12
MAR VIRGIN	8.2	.060	.124	.183	5
MAR LYRID	55	.044	.121	.223	9
HERCUL-LYR	200	.023	.073	.164	4
*TAU DRACO	990	.012	.043	.130	4
*PI DRACO	17	.050	.117	.186	6
*N VIRGIN	6.0	.060	.116	.168	10
*LIBRIDS	86	.025	.073	.143	4
LAM AURIG	12	.063	.140	.214	14
*APR VIRG	49	.045	.122	.222	5
NU HERCUL	120	.035	.105	.218	7
*ALPHA VIR	23	.038	.093	.153	9
EPS LYRID	79	.047	.135	.262	6
APR CYGNID	15	.086	.198	.310	16
*MAR ANDR	6.1	.084	.163	.236	12
O DRACONID	34	.053	.138	.237	7
GAMMA VIRG	190	.029	.091	.204	4
THETA LIBR	230	.021	.067	.155	3
*APR URSID	10	.083	.178	.268	15
G DRACONID	44	.029	.076	.139	3
ETA TAURID	52	.037	.101	.185	6
R DRACONID	20	.057	.137	.222	7
GAMMA PEG	3300	.013	.051	.194	5
MAY PISCID	130	.038	.115	.242	8
EPS ARIET	19	.059	.141	.226	11
*OMI CETID	430	.026	.088	.227	5
MAY ARIET	20	.154	.371	.599	-99
*S MAY OPH	73	.030	.085	.164	4
*N MAY OPH	3.7	.082	.141	.198	9
EPS AQUIL	53	.053	.145	.266	10
*MAY URSID	9.9	.072	.154	.232	15
MAY LYRID	49	.048	.131	.236	7
MAY DRACO	71	.031	.088	.168	6
MAY CASS	9.6	.052	.111	.166	5
*CHI SCORP	6.2	.080	.156	.226	13
JUNE CAMEL	180	.026	.081	.180	6
*ARIETIDS	12	.065	.144	.221	21
PSI AURIG	61	.033	.092	.172	5
JUNE AURIG	13	.045	.101	.156	5
*ZETA PERS	8.8	.155	.324	.483	90
M DRACONID	46	.045	.121	.218	6
*OPHIUCHID	32	.035	.090	.154	4
JUNE LYRID	60	.041	.114	.213	4
JUN CYGNID	33	.057	.147	.253	12
JUN AQUIL	48	.036	.098	.176	6
*SCOR-SGR	14	.077	.164	.255	16
ALP DRACO	2.0	.093	.133	.181	17
*SIGMA CAP	6.1	.062	.120	.174	9
*JUNE SCUT	11	.060	.131	.199	9
THETA AUR	22	.045	.110	.179	8
TAUR-ARIET	22	.053	.179	.211	9

STREAM	LAMBDA	SIGMA	DI	DII	NS
MU SAGIT	24	.042	.104	.171	7
AQUA-AQUIL	190	.020	.063	.141	5
CHI SAGITT	8800	.010	.041	.193	4
P DRACONID	90	.035	.102	.202	6
BOOT-DRACO	6800	.009	.037	.162	2
J DRACONID	23	.053	.130	.214	7
EPS CEPH	46	.047	.127	.228	7
BETA ANDR	640	.019	.066	.184	3
LACERTID	22	.064	.156	.255	12
OMEGA DRA	5.8	.147	.282	.407	65
CYGN-DRACO	18	.087	.206	.329	18
KAPPA PER	250	.025	.081	.189	5
KAPPA AUR	20	.042	.101	.163	3
*BETA TAUR	28	.037	.094	.157	6
TAU CAPRIC	15	.077	.177	.277	24
YPS DRACO	120	.032	.096	.199	6
SIGMA CASS	17	.059	.139	.220	10
JULY CEPH	75	.033	.094	.182	6
JULY CASS	52	.034	.093	.170	8
RHO DRACO	51	.042	.115	.209	7
KAPPA CASS	35	.044	.115	.198	6
CASSIOPEID	13	.066	.148	.229	17
J CEPHEID	420	.022	.074	.191	5
*JUL DRACO	29	.062	.158	.266	9
ZETA URSID	9.7	.061	.130	.195	13
PSI CASS	23	.059	.145	.238	11
CANES VEN	7.3	.091	.183	.269	17
OMI DRACO	57	.037	.102	.190	4
PI AQUARID	9.3	.093	.197	.294	21
*S DEL AQU	81	.041	.118	.230	37
A CEPHEID	18	.071	.168	.268	20
CEPH-DRACO	32	.054	.139	.238	9
OMI CEPH	24	.044	.109	.180	10
IODTA CEPH	28	.034	.086	.145	5
B CASSIOP	51	.040	.109	.199	7
GAMMA CEPH	5.3	.067	.126	.181	10
B CEPHEID	110	.027	.080	.165	6
IODTA CASS	13	.061	.137	.211	9
MU CANCRID	140	.024	.073	.156	8
O CAMELOP	930	.014	.050	.150	6
E DRACONID	18	.059	.140	.223	13
L DRACONID	110	.036	.107	.219	6
AUG LYNCID	11	.059	.129	.196	11
*AQU-CAPR	16	.076	.177	.279	22
*ALPHA CAP	3.5	.100	.169	.237	23
*S I AQUAR	50	.030	.082	.149	10
*BETA CEP	97	.032	.094	.189	6
C DRACONID	8.9	.092	.193	.288	26
AUG CASS	21	.053	.129	.209	16
GAMMA CYGN	98	.032	.094	.189	5
PERSEIDS	470	.026	.088	.232	3
GAMMA CASS	2400	.013	.050	.178	4
L CEPHEID	2.0	.144	.205	.280	41
AUG CEPH	13	.072	.162	.250	15
AUG DRACO	7.3	.085	.171	.251	30
AUG CANCR	11	.053	.116	.176	8
PHI DRACO	8.6	.073	.152	.226	23
AUG UMID	20	.050	.120	.194	13
E CAMELOP	9.7	.078	.166	.250	15
AUG URSIDS	100	.024	.071	.143	4
*N DEL AQU	9.1	.057	.120	.179	9
AUG CAMEL	9.2	.064	.135	.202	10
EPS URSID	10	.074	.159	.239	22
MU DRACO	2.3	.122	.182	.250	31
BETA URSID	8.0	.088	.181	.267	14
GAMMA LEO	3.1	.098	.161	.223	20
*N I AQUAR	4.1	.125	.221	.312	43
CASS-CEPH	54	.041	.113	.207	6
A CASSIOP	8.6	.082	.171	.254	11
XI LEONID	31	.054	.138	.236	12
OMEGA CASS	63	.033	.092	.174	9
E URSIDS	180	.027	.084	.187	4
F CAMELOP	18	.061	.145	.231	10
XI DRACO	2.2	.092	.135	.185	18
SEPT LYRID	2.3	.112	.167	.229	26
ALP TRIANG	62	.047	.131	.246	7
TAU LEONID	15	.073	.168	.263	16
D CEPHEID	9.3	.068	.144	.215	10
C CASSIOP	24	.055	.136	.224	7
RHO CEPH	210	.020	.063	.144	5
CASS-CAMEL	55	.035	.097	.178	6
CEPHEID	32	.049	.126	.216	19
BETA UMID	180	.025	.078	.173	6
C CAMELOP	110	.026	.077	.158	7
RHO URSID	35	.041	.107	.185	6

STREAM	LAMBDA	SIGMA	DI	DII	NS
B CAMELOP	14	.047	.107	.166	9
H CAMELOP	18	.060	.142	.227	11
ALP CAMEL	8.6	.058	.121	.180	9
SEPT URSID	90	.048	.140	.277	44
DRACO-UMID	13	.057	.128	.198	13
*ETA DRACO	15	.055	.127	.198	11
EPS UMID	5.0	.083	.154	.220	10
SEPT DRACO	6.6	.053	.105	.152	8
*PISCIDS	4.7	.075	.137	.195	25
SEPT CEPH	2.0	.132	.188	.256	31
ARIET-PISC	14	.060	.136	.212	16
*GAMMA PIS	44	.032	.086	.153	5
GAMMA ARIE	140	.032	.098	.208	6
ETA PERS	86	.037	.107	.211	6
XI CEPHEID	45	.034	.091	.164	5
RHO PISCID	170	.027	.084	.184	6
KAPPA CEPH	40	.040	.106	.187	12
F CEPHEID	57	.036	.100	.184	5
SEPT CASS	20	.052	.125	.202	9
D CASSIOP	580	.022	.076	.208	4
H CEPHEID	12	.067	.148	.227	8
GAMMA UMID	120	.029	.087	.181	4
D URSID	20	.046	.111	.179	5
SEPT CAMEL	32	.040	.103	.176	11
CAMELOPARD	7.1	.068	.136	.200	17
SEPT UMID	13	.059	.133	.205	9
A CAMELOP	660	.013	.045	.127	6
D DRACONID	10	.116	.249	.375	32
DEL PISCID	2.5	.106	.163	.224	23
OCT ANDROM	32	.043	.111	.189	7
OCT CEPH	8.1	.065	.134	.198	10
G CEPHEID	380	.020	.067	.169	5
*OCT DRACO	21	.055	.133	.217	18
K CAMELOP	56	.045	.124	.230	7
THET DRACO	3.1	.116	.190	.264	25
SEXTANTID	240	.037	.119	.277	5
L CAMELOP	38	.041	.108	.189	9
DEL URSID	90	.047	.137	.272	7
J CAMELOP	460	.023	.078	.204	6
*LAM DRACO	10	.094	.202	.303	20
A URSID	8.3	.118	.244	.362	33
N DRACONID	57	.031	.086	.159	4
G CAMELOP	19	.045	.108	.173	6
DRACO-CAM	7.8	.075	.153	.226	29
C URSID	20	.055	.132	.214	9
*S ARIETID	8.5	.128	.266	.395	99
PSI VIRGIN	11	.077	.168	.255	8
*ORIONIDS	76	.044	.126	.243	8
M CEPHEID	44	.041	.110	.196	5
E CEPHEID	330	.019	.063	.155	3
BETA CAMEL	190	.028	.088	.197	4
B URSID	51	.036	.098	.179	8
TAU URSID	27	.050	.126	.210	7
OCT URSID	8.5	.064	.133	.198	13
PSI DRACO	64	.032	.090	.169	8
B DRACONID	15	.051	.117	.184	9
OCT UMID	9.4	.045	.095	.143	4
ALP URSID	35	.043	.112	.194	10
A DRACONID	20	.057	.137	.222	14
OCT HERCUL	21	.049	.119	.193	10
*TAURIDS	8.0	.084	.173	.255	42
*TRIANGUL	11	.052	.113	.172	6
C CEPHEID	7.2	.054	.109	.159	5
GAMMA TAUR	32	.044	.113	.194	10
KAPPA DRAC	4.3	.074	.132	.187	11
EPS DRACO	20	.096	.231	.373	17
NOV ORION	250	.041	.132	.310	5
PHI TAURID	19	.084	.201	.322	23
IODTA AUR	66	.033	.093	.176	5
K CEPHEID	890	.018	.064	.190	3
*DRACO-URS	5.6	.079	.150	.216	19
NOV DRACO	14	.069	.157	.244	15
IODTA VIRG	9300	.010	.041	.196	3
F DRACONID	76	.035	.100	.193	10
NOV CAMEL	22	.055	.134	.219	11
SIG TAURID	160	.029	.090	.195	5
*MONOCERID	110	.036	.113	.232	14
K DRACONID	56	.039	.108	.199	6
*DEC DRACO	22	.048	.117	.191	12
*MU GEMINI	4.1	.128	.226	.319	41
*CHI ORION	9.6	.060	.170	.255	24
*GAMMA CAM	5.8	.100	.192	.277	19
*GEMINIDS	160	.040	.124	.269	75
DEC LYNCID	57	.036	.100	.184	5
*DEL DRACO	21	.047	.114	.185	7

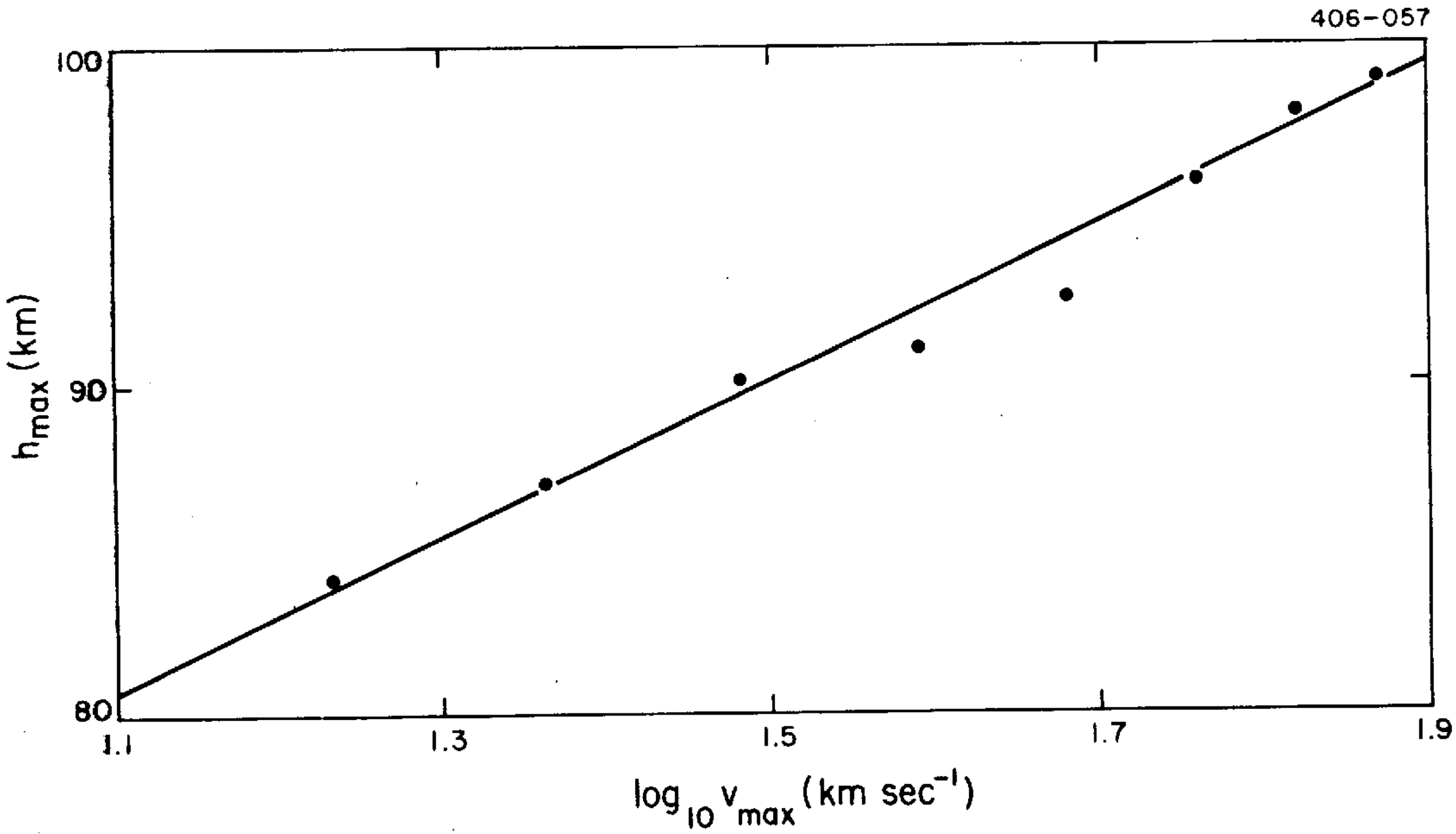

Figure 1. Mean heights at maximum ionization of 11061 meteors, with estimated corrections for diffusion.

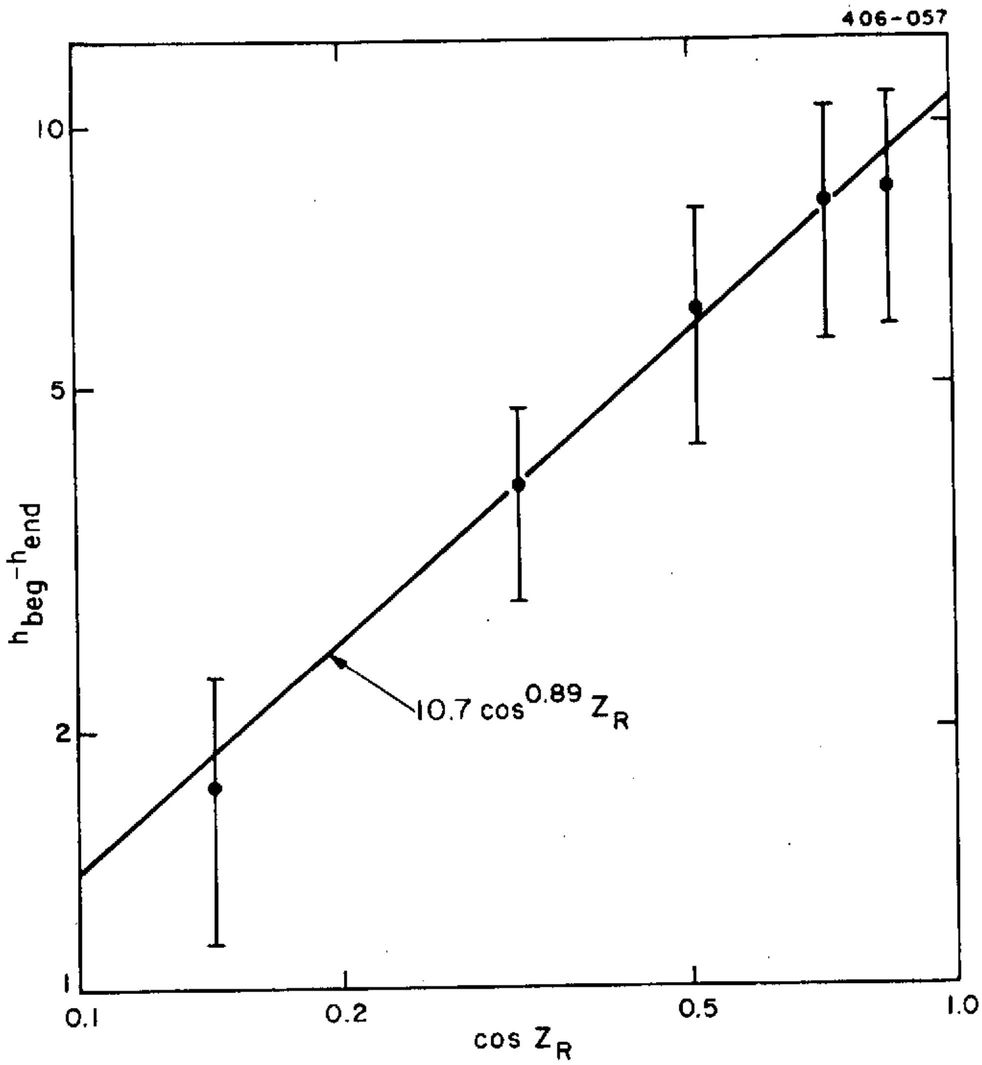

Figure 2. Vertical trail lengths and radiant zenith distances, from Table 5.

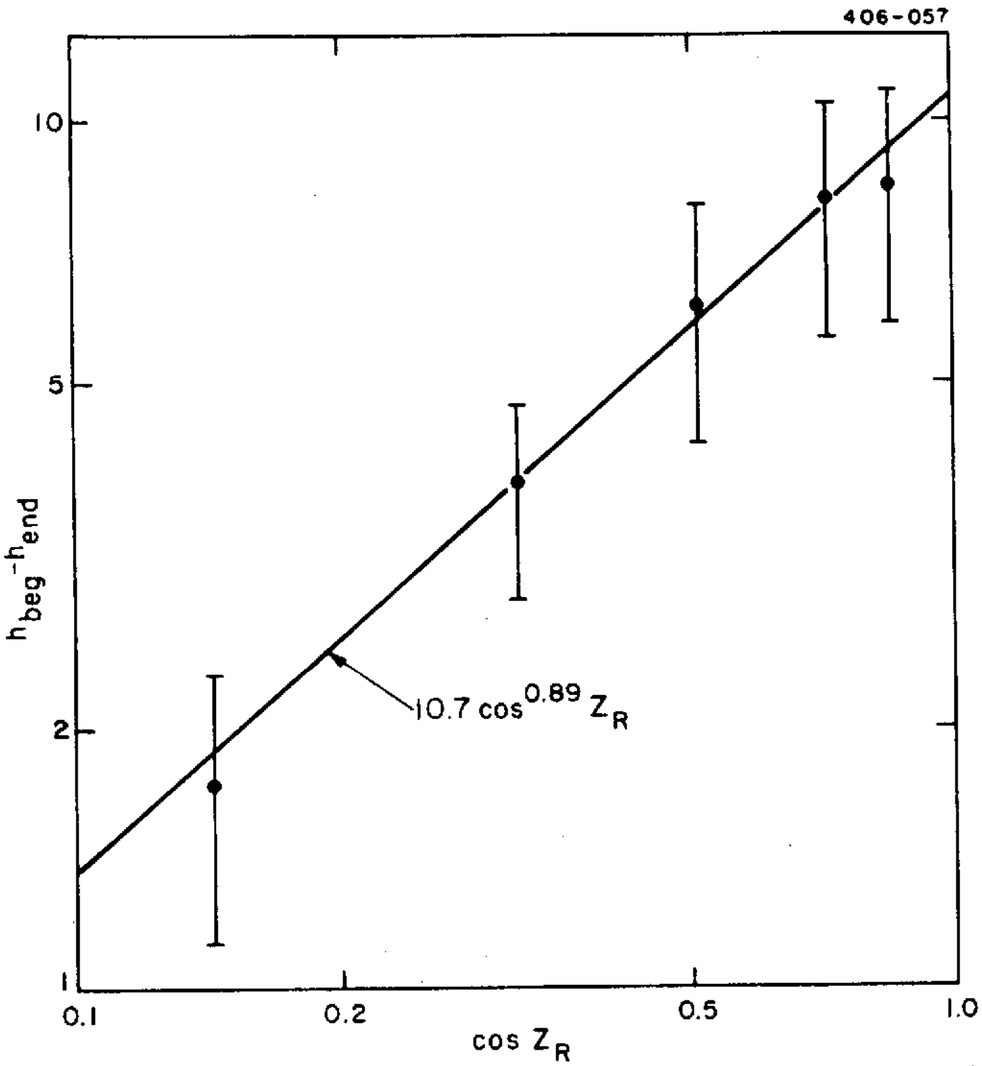

Figure 2. Vertical trail lengths and radiant zenith distances, from Table 5.